Measurement and Prediction of the Elongational Stress Growth in a Dilute Solution of DNA Molecules

P. Sunthar, Duc At Nguyen, Roelf Dubbelboer,† J. Ravi Prakash,* and Tam Sridhar

Department of Chemical Engineering, Monash University, Melbourne VIC 3800, Australia

Received June 7, 2005; Revised Manuscript Received September 9, 2005

ABSTRACT: We report the measurement of the elongational stress growth coefficient of a dilute solution of λ-phage DNA molecules in sugar and corn-syrup solvent mixtures under excess salt conditions. The stress growth is measured using a filament stretching rheometer, at strain rates far exceeding the inverse relaxation time of the DNA molecule. The DNA molecule is assumed to behave like a long chain polymer molecule under good solvent conditions, and the observed behavior is modeled using a bead−spring chain model for the DNA. Excluded-volume (EV) effects are accounted for by a narrow-Gaussian repulsive potential between the beads, hydrodynamic interactions (HI) between beads are approximated by the Rotne−Prager−Yamakawa tensor, and the finite length of the DNA molecule is treated by springs whose force−extension behavior mimics that of a wormlike chain. By combining a Brownian dynamics simulation of the chain along with the recently introduced method of successive fine graining [Sunthar, P.; Prakash, J. R. *Macromolecules* **2005**, *38*, 617], predictions of the stress growth coefficient are obtained which are insensitive to the microscopic interaction parameters for EV and HI.

1. Introduction

Experiments on a dilute solution of DNA molecules subjected to flow are of interest in validating statistical theories of long chain polymer molecules,[1] in general, and for the design of microfluidic devices[2,3] such as those used for DNA size separation, in particular. Predominantly to date, experiments in elongational flows[4,5] have been conducted in cross slot cells and the various conformations adopted by the DNA molecules have been observed under a microscope. The observed behavior has been successfully predicted by invoking theoretical descriptions of dilute polymer solutions.[6−8] However, with stagnation point flow devices such as the cross slot cell, it is not possible to obtain the true elongational viscosity of the solution; only an effective elongational viscosity can be obtained due to the nonuniform residence time of the molecules, as they pass through the device.[9] A filament stretching rheometer (FSR) is commonly believed to be the best way to obtain reliable estimates of the elongational stress of a polymer solution.[10] We report the measurement of the stress growth (from equilibrium to steady state) of a dilute solution of λ-phage DNA molecules subjected to uniaxial elongational flow in an FSR. We also apply our earlier theoretical treatment[8] using a bead−spring chain model for the DNA molecule to predict the stress growth.

In a filament stretching rheometer, a polymer solution sample is placed between two plates initially at rest, which are subsequently moved apart at a controlled exponential rate. This generates a stretching liquid bridge undergoing a constant strain rate uniaxial elongational flow near its midpoint.[11,12] The force required to bring about the separation is dependent, among other factors, on the stress due to the polymers being extended from their equilibrium coillike shape to extended shapes. The stress is obtained by measuring this force at one of the end plates and the midpoint diameter of the filament.[13] By carefully choosing a solvent and an extension rate, it is possible to isolate the polymer contribution to the stress from other factors such as gravity, surface tension, and inertia.[10] The FSR procedure has been standardized[14] to remove various nonidealities in the flow kinematics[15] and provides the most reliable measurement of the elongational stress of a dilute polymer solution currently available. McKinley and Sridhar[10] have recently presented a review of the filament stretching rheometry. The extensional rheology of dilute solutions of polystyrene at various concentrations and molecular weights is one of the most well-studied systems using the filament stretching rheometer.[16] While dilute solutions of stained DNA have been used to study the behavior of the conformations in shear[17,18] and extensional flows,[4,5] the present study is the first to quantify the elongational stress of such solutions using the FSR.

The theoretical treatments of the rheology of dilute polymer solutions start with a mechanical model for the polymer molecule, such as the bead−spring chain model, subject to various solvent forces. The behavior of the solution subject to flow is obtained by writing a kinetic equation for the distribution function of the bead positions and momenta. The macroscopic observables, such as the mean size of the polymer or the stress due to it, can be obtained from the distribution function by taking suitable averages using the standard methods of statistical mechanics.[19] It is currently understood that a realistic model requires the incorporation of solvent-mediated hydrodynamic interactions (HI) between the beads, finite length extensibility of the spring, and excluded-volume (EV) interactions.[20] While simplified models, such as Zimm's treatment using linear (Hookean) springs with preaveraged HI,[21] provide closed form solutions for the macroscopic observables, the inherent assumptions become invalidated in strong flows. The behavior of the model with all the above nonlinearities can be examined by using a Brownian dynamics simu-

† Presently at Orica Australia Pty. Ltd, Melbourne, Australia.
* To whom correspondence must be addressed. E-mail: Ravi.Jagadeeshan@eng.monash.edu.au.

10.1021/ma0511907 CCC: $30.25
Published on Web 10/27/2005

lation (BDS) of the polymer chain which provides an "exact" solution (within simulation error bounds) to the governing equations. BDS have been carried out for DNA and polystyrene systems subject to extensional flow and quantitative agreements with experiments were obtained.[6,7] However, this agreement was obtained only by using different kinds of parameter fitting procedures. As has been discussed previously in ref 8, fitting the model interaction parameters for EV and HI is necessary when a bead−spring chain model with a finite number of beads N is used. A procedure termed successive fine graining (SFG) has recently been introduced by Sunthar and Prakash[8] and Prabhakar et al.[22] by which exact parameter determination at finite N is circumvented. In the SFG procedure, a polymer of finite length is represented by an increasingly larger number of beads N, with the model interaction parameters chosen arbitrarily initially and subsequently modified by a systematic procedure, as described in ref 8, as N is increased. The quantities of interest obtained from the model (in equilibrium or in flow) are then extrapolated to the limit $(N - 1) \rightarrow N_k$, where N_k is the total number of Kuhn segments in the polymer chain. For sufficiently large N_k, it was shown that the macroscopic equilibrium properties of the chain are truly independent of the microscopic interaction parameters for EV and HI.[8] A similar behavior is seen with respect to flow properties, except that they are now insensitive to the interaction parameters in a range of values. This was demonstrated in the cases of the average stretch of DNA in elongational flow[8] and the elongational viscosity of polystyrene solutions.[22] In ref 22, excluded-volume interactions were ignored as the polystyrene solution was assumed to be at its θ-temperature. While the present work has similar goals as ref 22, viz., to predict the growth of elongational viscosity (or the stress growth coefficient), here excluded-volume effects are included as they have been shown to be crucial to obtain an accurate description of DNA solutions of the kind used in the present experiments.[8]

Excluded-volume effects become important in flexible polymers when monomer segments, though distant along a chain, interact to repel each other as they come close to each other in space. This interaction, which is absent in ideal chains obeying Gaussian statistics (or at θ conditions), leads to a swelling of the polymer size[1] and modifies both equilibrium and rheological properties. In the case of DNA solutions, the charged backbone of the DNA leads to long-range interactions, and as a result the molecule is normally not flexible; however, in the presence of excess salt the electrostatic repulsion is screened,[23] leading to an effective short-ranged repulsion. The DNA chain is then expected to behave like a neutral polymer in a good solvent. To obtain quantitative agreement of the behavior of DNA molecules under flow, therefore, EV interactions need to be incorporated. In this work we predict the elongational stress growth of a dilute solution of DNA molecules in terms of a well-studied equilibrium measure of EV effects, namely the solvent quality parameter z. The procedure adopted here is based on the method introduced recently in ref 8.

The solvent quality parameter z is defined as

$$z = v_0 (1 - T_\theta/T) \sqrt{M} \tag{1}$$

where T is a temperature above the θ-temperature T_θ, M is the molecular weight of the polymer, and v_0 is a chemistry-dependent constant. z represents a scaling variable that can be used to describe the crossover from ideal chain molecular weight scaling to the scaling observed in a good solvent. Thus, certain ratios of equilibrium properties of various polymer−solvent systems at various temperatures can be collapsed onto an unique master curve as a function of z, by suitably choosing the chemistry-dependent proportionality constant v_0 in the above relationship.[24,25] The value of z reflects the "goodness" of the solvent, as it goes from $z = 0$ (theta) to $z \rightarrow \infty$. The significance of using z to characterize polymers in good solvents is elucidated by the two-parameter theory, which states that the static and dynamic properties of a long chain polymer are determined by just two parameters, namely, the radius of gyration of the chain at θ-conditions R_g^θ and the solvent quality z.[26] The two-parameter theory has been extensively studied using renormalization group calculations of EV interactions.[27]

While the understanding of EV effects on the scaling of equilibrium properties is at an advanced level, such rigor has not yet been attained in the study of rheological properties. Numerous groups[6,28−33] have used molecular simulations of models such as bead−spring or bead−rod chains to study the influence of EV interactions on elongational flow properties. EV interactions between the beads are typically incorporated by using Lennard-Jones-like potentials or by purely repulsive potentials, such as a Gaussian potential. In the absence of studies to link the parameters in these models to the solvent quality parameter z, the powerful results of the two-parameter theory cannot be used, and to compensate for it, one or more parameters in the interaction potential need to be fitted to match a restricted choice of equilibrium properties.

With a Gaussian EV potential,[34] however, it is easy to relate the solvent quality for small values of z to the model parameter z^* through $z = z^*\sqrt{N}$, where z^* is the strength of the potential and N is the number of beads in the chain.[35,36] Recently, it was shown using exact calculations with BDS that this relationship for a Gaussian potential is valid even for large values of z, and the experimentally observed swelling of the radius of gyration[24] can be accurately predicted.[37] The treatment in ref 37, which was restricted to chains with Hookean (linear) springs, was extended by Sunthar and Prakash[8] to springs obeying more general force laws, such as FENE and wormlike force laws, and it was shown that the interaction potential is rescaled by the average equilibrium length of a single spring χ, so that $z = (z^*/\chi^3)\sqrt{N}$. Since the whole methodology was developed in the context of BDS, it becomes possible for the first time to include fluctuating hydrodynamic interactions and to study the influence of EV interactions in flow using a value for the solvent quality z that can be uniquely determined from experimental measurements at equilibrium. In ref 8 this procedure was applied to predict the evolution of the stretch of λ-DNA in elongational flow reported by Smith and Chu.[4] The effect of the equilibrium solvent quality was shown to have a pronounced effect on the rate at which the λ-DNA molecule unravelled from a coil to a stretched state under elongational flow. In the present work, a similar procedure is applied to predict the elongational stress growth of λ-DNA and to examine the influence of solvent quality on the predictions.

The experimental methodology and the solutions used here are described in section 2. The model details, the

Table 1. Main Components of the Solvents Used in This Work

label	sucrose (wt %)	corn syrup (wt %)	water (wt %)
DNA-2	22.3	45.8	32.1
DNA-5	61.2	0	38.8

equations governing its dynamics, the simulation methodology, and the method of successive fine graining are reviewed in section 3. The measured elongational stress growth of λ-DNA in sugar-corn syrup solutions, theoretical predictions, and the role of solvent quality are discussed in section 4.

2. Materials and Experimental Methods

We have conducted elongational flow experiments on several solutions of λ-DNA to simultaneously observe the conformational behavior of λ-DNA and measure the stresses developed by the solution. However, in this article we report the measurements of the elongational stress growth coefficient in only two of these solutions. The two fluid samples studied in this work, labeled DNA-2 and DNA-5, were prepared by dissolving a small amount of λ-DNA (New England Biolabs, procured as a solution of 0.5 mg/mL) in two buffer solvents. (The solution also consisted of a small amount of fluorescently stained λ-DNA, using the dye YOYO-1 from Molecular Probes Inc., to enable its conformational measurement, the results of which will be published elsewhere—they are not directly relevant to the study reported in this publication.) The solvents mainly consist of saturated sucrose (at 21 °C) and corn syrup in varying proportions as indicated in Table 1. The buffer solution consists of 2 mM EDTA, 10 mM NaCl, 10 mM Tris HCl (pH = 8), 50 μg/mL glucose oxidase, and 10 μg/mL catalase (both from Boehringer Mannheim Gmbh, Germany) and 4 vol % β-mercaptoethanol to prevent the stained λ-DNA from photobleaching.[38]

λ-DNA has a linear double-stranded helical structure, containing 48 502 basepairs (with a molecular weight of 650 g/mol per basepair), leading a total molecular weight of $M \approx 31.5 \times 10^6$. The contour length of unstained λ-DNA is $\approx$16.5 μm, and staining increases it to $\approx$22 μm. Thus, the solution is not strictly monodisperse. However, since the λ-DNA concentrations are such that the ratio of stained to unstained λ-DNA is nearly 1:850, we assume that the contribution to the solution stress from λ-DNA is mainly from the unstained λ-DNA.[40]

The physical and linear viscoelastic properties of the two solutions are tabulated in Table 2. The polymer contribution to the zero shear viscosity (η_p) was obtained from a oscillatory shear experiment, in the limit of zero frequency of oscillation. This provides a means to obtain a characteristic relaxation time of the λ-DNA molecules and also characterize the diluteness of the solution. We have also conducted shear experiments in a solution similar to DNA-2, but with a lower λ-DNA concentration of $c \approx 20$ μg/mL. This gives $\eta_p/(c\eta_s)$ of $\sim$0.0221 mL/μg. Together with the data shown in Table 2, this suggests that the λ-DNA solution considered in this work can be considered dilute, since there is no variation in the value of $\eta_p/(c\eta_s)$ with concentration. We therefore take the intrinsic viscosity to be $[\eta]_0 = 0.023 \pm 0.001$ mL/μg, obtained by taking an average of the three measured zero shear rate viscosities. (In arriving at this value, it has been assumed that the various solvents considered here have the same solvent quality for λ-DNA and vary only in their viscosities. Some justification for this assumption can be seen in Figure 5, where the measured elongational viscosity does not show any appreciable difference across the solvents.) The argument that the solutions are dilute is also consistent with a recently reported theoretical estimate of the radius of gyration of λ-DNA in a similar solution. In ref 8, a value for the radius of gyration of unstained λ-DNA in the solution considered in ref 4 was suggested to be around 0.608 μm (at a solvent quality $z = 1$; these calculations are also given in section 4.3). This gives a overlap concentration of $c^* = 55.6$ μg/mL, which is well above the concentrations of λ-DNA considered in the present work. Note that the solution used in ref 4 was also a sugar solution, similar to the DNA-5 solution considered here.

It is possible to define a characteristic relaxtion time of λ-DNA in the solution obtained from the intrinsic viscosity. The relaxation time is defined as

$$\lambda_\eta \equiv \frac{[\eta]_0 M}{N_A} \frac{\eta_s}{kT} \tag{2}$$

where N_A is the Avogadro number and k is the Boltzmann constant. All experiments were carried out at a constant temperature of 21 $\pm$ 0.5 °C. The characteristic relaxation time obtained this way is also shown in Table 2.

The elongational stress growth coefficient (or the extensional viscosity) of the two solutions was obtained using the filament stretching rheometer (details of which have been published earlier in refs 41 and 14) for various strain rates by a "master curve" technique.[16] The strain rates for the extension were chosen such that an uniform extension of the filament was obtained. Since the DNA-5 solution has a low zero shear viscosity, a high strain rate of around 50 s^{-1} was required to prevent the gravitational sagging of the filament as it was being stretched. Under these conditions, the variation of midpoint diameter could no longer be tracked by the standard laser technique used in our FSR assembly.[16] Alternatively, the midpoint diameter of the filament was calculated from a video recording using a high-speed digital camera (Phantom 5 from Vision Research, Inc.), which is capable of handling up to 1000 frames/s. Additionally, to enhance the signal-to-noise ratio for the low values of stresses measured, the force transducer was kept stationary on the top plate of the FSR (only the bottom plate was subjected to motion). The inertial contribution to the stress, calculated using Szabo's equation,[42] was found to be negligible even at this high strain rate. The strain rates used for the experiments are shown in Table 2. The strain rates therefore far exceed the characteristic inverse relaxation time (λ_η^{-1}).

3. Model and Simulation Method

3.1. Governing Equations. In this work a dilute solution of DNA molecules is modeled as an ensemble of noninteracting bead−spring chains, each of which has N spherical beads (which act as centers of hydrodynamic resistance) connected by massless springs representing an entropic force between two points on the polymer chain. The equations governing the motion of the beads is written as a stochastic differential equation, equivalent to a Fokker−Planck equation for the time evolution of the probability distribution function of the configuration of the bead positions.[19,43] In this paper we will use index (or indicial) notation using subscripts to denote vectors and tensors; a Greek subscript μ, ν, ... = [1, 2, ..., N] will denote the bead index, and a Roman subscript i, j, ... = [1, 2, 3] will denote the Cartesian coordinate index. The displacement of a bead position $\Delta R_{\mu i}$ during a finite time increment Δt, correct to $\mathcal{O}(\Delta t)$, is given by[33]

$$\Delta R_{\mu i} = \kappa_{ij} R_{\mu j} \Delta t + \frac{1}{4} D_{\mu\nu ij} F_{\nu j} \Delta t + \frac{1}{\sqrt{2}} B_{\mu\nu ij} \Delta W_{\nu j} \tag{3}$$

where the summation convention is implied for repeated indices. In the above equation, $R_{\mu i}$ is the bead position vector matrix, κ_{ij} is the time-dependent, homogeneous, velocity gradient tensor of the surrounding fluid motion, $D_{\mu\nu ij}$ is the diffusion tensor, $F_{\mu i}$ is a matrix of the total body force acting on the beads, $B_{\mu\nu ij}$ is taken as the square root matrix of $D_{\mu\nu ij}$ defined as $B_{\mu\theta ik} B_{\nu\theta jk} \equiv D_{\mu\nu ij}$, and $\Delta W_{\mu i}$ is an increment to the Weiner process $W_{\nu j}$ such that the elements of the matrix $\Delta W_{\nu j}$ are Gaussian

Table 2. Physical and Linear Viscoelastic Properties of the Two Fluid Samples Measured at 21 °C[a]

sample	c (μg/mL)	ρ (g/mL)	η_p (Pa s)	η_s (Pa s)	$\eta_p/(c\eta_s)$ (mL/μg)	λ_η (s)	$\dot{\epsilon}$ (s^{-1})
DNA-2	35.9	1.36	0.31	0.37	0.0233	109	5.6−20.6
DNA-5	35.6	1.30	0.049	0.058	0.0237	17	53.4

[a] c is the concentration of λ-DNA, ρ is the mass density of the solution, η_p is the polymer contribution to the zero shear rate viscosity of the solution, η_s is the viscosity of the solvent, and λ_η is a relaxation time obtained from the intrinsic viscosity, defined in eq 2. The strain rates ($\dot{\epsilon}$) used for the elongational stress measurement are also indicated here.

distributed with zero mean and variance Δt. All the lengths have been scaled by the equilibrium length of a single linear spring $l_H = \sqrt{kT/H}$, times have been scaled by $\lambda_H = \zeta/4H$, and energy has been scaled by kT. In these expressions, H is the linear spring constant and $\zeta = 6\pi\eta_s a$ is the Stokes friction coefficient of a spherical bead of dimensional radius a in a solvent of viscosity η_s.

One of the contributions to the total body force F_{vj} acting on a bead arises from the net entropic spring force (F^s_{vj}) due to the connector forces from the springs adjacent to a bead: $F^s_{vj} = F^c_{vj}(Q_{vj}) - F^c_{v-1j}(Q_{v-1j})$, where $Q_{vj} = R_{v+1j} - R_{vj}$ is the matrix of connector vectors between adjacent beads. For DNA a commonly employed spring model is one that mimics a wormlike chain (WLC) force−extension behavior. It is written as an interpolatory formula between the limits of the Hookean force regime and the regime close to the full extension.[44] This provides a finite length extensibility to a single spring and by implication to the chain of springs. The connector force of a WLC spring with a connector vector Q_i is given by

$$F^c_i = Q_i \frac{1}{6q}\left(4q + \frac{1}{(1-q)^2} - 1\right) \tag{4}$$

where $q \equiv \sqrt{Q_i Q_i}/\sqrt{b}$ is the magnitude of the connector vector normalized by the fully stretched length. Here, b is the square of the fully stretched length of a single spring. The second contribution to the body force comes from the pairwise excluded-volume interaction between the beads. Here we use the force derived from a narrow-Gaussian repulsive potential.[34] The EV force between two beads connected by the vector r_i is given by

$$F^e_i(r_i) = \frac{z^*}{d^{*5}} e^{-r^2/2d^{*2}} r_i \tag{5}$$

where $r \equiv \sqrt{r_i r_i}$ is the magnitude of r_i. The EV force above is parametrized by z^*, a nondimensional volume representing the strength of EV interactions, and d^*, a characteristic length of the range of interactions. The total body force on a bead μ is therefore given by $F_{\mu i} = F^s_{\mu i} + \sum_{\nu=1}^{N} F^e_i(r_{\mu\nu i})$, where $r_{\mu\nu i}$ is a tensor of connector vectors between beads with indices μ and ν.

We assume solvent-mediated hydrodynamic interactions (HI) to be present between the beads. The diffusion tensor in this case is $D_{\mu\nu ij} = \delta_{ij}\delta_{\mu\nu} + \Omega_{\mu\nu ij}$, where δ_{ij} is the Kronecker delta and $\Omega_{\mu\nu ij} = \Omega_{ij}(r_{\mu\nu i})$ is taken to be the regularized Rotne−Prager−Yamakawa (RPY) HI tensor,[45] whose functional form is given by

$$\Omega_{ij}(r_i) = \left[\Omega_1 \delta_{ij} + \Omega_2 \frac{r_i r_j}{r^2}\right] \tag{6}$$

where for $r \geq 2\sqrt{\pi}h^*$

$$\Omega_1 = \frac{3\sqrt{\pi}}{4}\frac{h^*}{r}\left(1 + \frac{2\pi}{3}\frac{h^{*2}}{r^2}\right), \qquad \Omega_2 = \frac{3\sqrt{\pi}}{4}\frac{h^*}{r}\left(1 - 2\pi\frac{h^{*2}}{r^2}\right) \tag{7}$$

while for $0 < r \leq 2\sqrt{\pi}h^*$

$$\Omega_1 = 1 - \frac{9}{32}\frac{r}{h^*\sqrt{\pi}}, \quad \Omega_2 = \frac{3}{32}\frac{r}{h^*\sqrt{\pi}} \tag{8}$$

In eq 3, the square root matrix B is obtained using a Chebyshev polynomial approximation of the square root function, originally proposed by Fixman[46] and recently refined with an iterative scheme to maintain the accuracy of the approximation.[47] The stochastic differential equation is solved using a semiimplicit iterative scheme at each time step.[33] Averages of the configuration-dependent properties are obtained by simulating a large ensemble of trajectories. Each of the trajectories is started by sampling the initial configuration from the known distribution function at θ-conditions.[19] It is then equilibriated without the flow field to the given solvent conditions (with HI ignored for faster computation). This is followed by subjecting it to an uniaxial elongational flow field. The velocity gradient tensor in this case is given by

$$\kappa_{ij} = \dot{\epsilon}^* \begin{pmatrix} 1 & 0 & 0 \\ 0 & -\frac{1}{2} & 0 \\ 0 & 0 & -\frac{1}{2} \end{pmatrix} \tag{9}$$

where $\dot{\epsilon}^*$ is the (scaled) strain rate. For the simulations with flow, a time increment of $\Delta t = 0.01$ was used which provided a converged solution for the ensemble averages.

It is appropriate to introduce some definitions at this point that will be used in the following sections. For the model described above the mean equilibrium radius of gyration at θ-conditions is given by

$$R_g^{\theta *} = \chi\sqrt{\frac{N^2 - 1}{2N}} \tag{10}$$

where $\chi = \chi(b)$ is the characteristic equilibrium length of a single spring, defined by

$$\chi^2(b) = \frac{\langle Q_i Q_i \rangle}{3} \tag{11}$$

where Q_i is the end-to-end vector for a single spring with a given value of b. χ needs to be evaluated numerically in the case of a WLC spring-force model, as shown in the Appendix B of ref 8. The fully stretched length is given by

$$L_0 = (N-1)\sqrt{b} \tag{12}$$

A useful way to represent the ratio of these two length measures is the number of Kuhn steps (or Kuhn statistical segments) N_k, defined as

$$N_k \equiv \frac{{L_0}^2}{6(R_g^{\theta*})^2} \tag{13}$$

3.2. Parameter Values and Successive Fine Graining. To be able to simulate a given DNA chain, the model parameters N, b, h^*, z^*, d^*, l_H, and λ_H need to be identified.[8] The procedure commonly adopted is to choose the parameters such that the model reproduces certain measured equilibrium properties of the DNA chain. Except for some simplified cases, such as that of a chain of Hookean springs ($b \to \infty$) at θ-conditions (z^*, $d^* = 0$), it is tedious to estimate the parameters for a finite N model. Even if one such parameter set is found, such as the one chosen in ref 6 for λ-DNA in a sugar solution, it is not guaranteed that the predictions in flow will correspond to that of the DNA molecule. For example, in ref 5 it was reported that while the suggested combination of parameters worked well in some cases, it led to poor predictions in others. With this procedure of parameter selection it is also not clear (i) how many experimental measurements are required to fix the model parameters and (ii) whether any other combination of the model parameters will not reproduce the same predictions. The successive fine graining (SFG) procedure suggested in ref 8 is able to overcome these difficulties and uncertainties.

In the SFG method, the only experimental measurements concerning the polymer that are required are that of (i) the equilibrium radius of gyration at θ-conditions R_g^θ, (ii) the solvent quality z, and (iii) the fully stretched length. Provided these data, the parameters b, z^*, and l_H of the model can be easily determined for any choice of N. The model interaction parameters h^* and d^* are initially chosen arbitrarily (this also fixes λ_H). The behavior exhibited by the model in equilibrium, such as the relaxation time, for this choice is recorded. The number of beads in the model is then progressively increased, keeping the following model properties invariant: (i) R_g^θ, (ii) L_0, (iii) solvent quality z, and (iv) rescaled HI parameter $\tilde{h}^* = h^*/\chi$. Using a suitably chosen variable, such as one of the equilibrium universal ratios,[8,48] the data recorded for that variable for various values of N are then extrapolated to the limit $N \to \infty$. In this limit the model predictions for the ratios become insensitive to the initially made choice of h^* and d^* (thereby eliminating two parameters from the model), and the correct solvent quality limit is attained. As outlined in the Introduction, and elaborated in ref 8, this automatically matches with all the static and dynamic properties of the chain at equilibrium.

To study the properties under flow, in addition to the invariants listed above, the Weissenberg number, defined as $Wi = \lambda\dot{\epsilon}$, where λ is any characteristic relaxation time of the molecule, is kept invariant as N is progressively increased. A ratio constructed from the variable of interest (such as the stretch or the viscosity) is used to extrapolate the finite N data. In this case, however, the finite N data are extrapolated to the limit $(N-1) \to N_k$ because of the dependence of the flow properties on the finite length of the chain.[8,22]

Since we are interested in predicting the extensional stress growth, we carry out the extrapolations in the variable $U^+_{\bar{\eta}R}$, defined as

$$U^+_{\bar{\eta}R} \equiv \frac{[\bar{\eta}]\, M/N_A}{\frac{4}{3}\pi {R_g}^3} \tag{14}$$

where R_g is the dimensional radius of gyration at equilibrium at the given solvent conditions and $[\bar{\eta}]$ is defined as an "intrinsic extensional viscosity"

$$[\bar{\eta}] \equiv \lim_{c\to 0} \frac{\bar{\eta}_p}{c\eta_s} \equiv \lim_{n_p \to 0} \frac{\bar{\eta}_p N_A/M}{n_p \eta_s} \tag{15}$$

where $\bar{\eta}_p$ is the polymer contribution to the elongational viscosity (or the stress growth coefficient) and n_p is the polymer number density. In terms of nondimensional model variables, eq 14 can be written as

$$U^+_{\bar{\eta}R} = \frac{9}{8}\sqrt{\pi} h^* \frac{\bar{\eta}^*}{{R_g}^{*3}} \tag{16}$$

The theoretical value for the polymer contribution to the elongational viscosity $\bar{\eta}^*$ can be obtained from simulations by calculating the ensemble average of the normal stress difference[19]

$$\bar{\eta}^* \equiv -\frac{\tau_{11} - \tau_{22}}{\dot{\epsilon}^*} \tag{17}$$

where the nondimensional stress tensor τ_{ij} is obtained from the Kramers−Kirkwood expression[19]

$$\tau_{ij} = \langle S_{ij} \rangle \equiv \langle F_{\mu i}(R_{\mu j} - \bar{R}_j) \rangle \tag{18}$$

with $\bar{R}_j = \sum_\mu R_{\mu j}/N$ being the position vector of the center of mass of the beads in the chain. Experiments usually measure the extensional viscosity of the solution $\bar{\eta}$ such that

$$\bar{\eta} = 3\eta_s + \bar{\eta}_p \tag{19}$$

Assuming that the limit in eq 15 is obeyed, we have the ratio $U^+_{\bar{\eta}R}$ as measured through experiments given by

$$U^+_{\bar{\eta}R} = \frac{\bar{\eta} - 3\eta_s}{n_p \eta_s \frac{4}{3}\pi {R_g}^3} \tag{20}$$

4. Results and Discussion

4.1. Parameter-Free Predictions. Before applying the SFG method to predict the elongational stress growth of the DNA solutions investigated here, we first study the influence of solvent quality within the model framework. The nondimensional model requires only two parameters to be determined from experiments:[8] the effective Kuhn segments N_k (see eq 13) and the solvent quality z. In the discussions below we assume $N_k = 200$, as used in ref 8 for λ-DNA, and consider various solvent qualities.

A detailed algorithmic procedure to calculate the values of the parameters in the model for a given value of N is given in ref 8. Briefly, various values of N, spaced uniformly on a $1/\sqrt{N}$ space, are chosen first. The value of b and χ are calculated for each of these values for $N_k = 200$ (see Table 3). The rescaled HI parameter $\tilde{h}^*$ is kept constant as N is changed. Simulations are carried

Table 3. Parameter Values for the WLC Springs Used in the SFG Scheme for $N_k = 200$[a]

N	15	17	19	23	27	33	41	51
b	35.53	29.97	25.72	19.66	15.56	11.43	7.947	5.246
χ	0.8837	0.871	0.8584	0.8333	0.8082	0.7704	0.719	0.6531

[a] The procedure and expressions used to obtain them are given in ref 8.

out for two values of $\tilde{h}^*$ chosen arbitrarily: $\tilde{h}^* = \{0.19, 0.30\}$. The HI parameter h^* for the simulation is obtained at each N from

$$h^* = \chi \tilde{h}^* \tag{21}$$

Three different solvent qualities are considered: $z = \{0, 1, 3\}$. For each of them, the parameters of the EV potential are obtained from

$$z^* = z\chi^3/\sqrt{N} \tag{22}$$

$$d^* = Kz^{*1/5} \tag{23}$$

To ensure that the extrapolated result is independent of d^*, two values of K are used: $K = \{1.0, 1.5\}$

To keep the Weissenberg number Wi constant as the chain is successively fine grained, it is essential to determine a characteristic relaxation time for the chosen set of parameters at each value N. In the earlier work[8] a longest relaxation time λ_1, as determined by the relaxation of initially stretched molecules, was used. Here, we propose to use a nondimensional relaxation time λ_η^* obtained from the zero-shear rate intrinsic viscosity $[\eta]_0$, as given in eq 2:

$$\lambda_\eta^* = \frac{\lambda_\eta}{\lambda_H} \tag{24}$$

The intrinsic viscosity is obtained from the simulations by using a Green−Kubo formula for the autocorrelation function of the stress.[49,50] The relaxation time is then given by

$$\lambda_\eta^* = \int_0^\infty \mathrm{d}t\, C_S(t) \equiv \frac{1}{6}\sum_{i\neq j}\int_0^\infty \mathrm{d}t\, \langle S_{ij}(0)\, S_{ij}(t)\rangle_{eq}^{\dagger} \tag{25}$$

The tensor S_{ij} is defined in eq 18. Note that in the tensor product the sum is taken only over all $i \neq j$ and averaged over them. This is permitted because of the spatial symmetry of the average at equilibrium. A superscript † is affixed over $\langle\cdot\rangle$ to indicate that the equilibrium average may be either an ensemble average over a single time interval t or a time average over several instances separated by t. In this work, the autocorrelation function $C_S(t)$ is found using the algorithm suggested in ref 51, by carrying out equilibrium simulations of a few trajectories but each extending to about $\mathcal{O}(10^4\lambda_{1,Zimm})$, where $\lambda_{1,Zimm}$ is the longest Zimm relaxation time obtained for a model with the same h^* and N, but with Hookean springs.

In the preaveraged model (such as that of Zimm) $C_S(t)$ decays through a discrete spectrum of relaxation times. Though in the case of fluctuating HI, the spectrum may not be discrete, it is convenient to fit a discrete spectrum to the time-correlation function to evaluate the integral of eq 25. One of the ways to fit a weighted sum of exponentials

$$C_S(t) = \sum_{i=1}^{m} a_i \mathrm{e}^{-t/\lambda_i} \tag{26}$$

to the data is the graphical (or "peeling") method.[52] Since we are interested only in the integral rather than the spectrum, the peeling method with a suitable choice of the number of modes m is the simplest means of obtaining the multiexponential fit. The method was validated with a known discrete Zimm spectrum of 19 modes, by fitting a multiexponential with just $m = 4$ modes. (In the peeling method, the number of modes required to represent the function is not known a priori, but rather determined as a part of the solution.) The error in the integral when compared to the known value was less than 0.1%. For the stress correlation obtained by fitting the actual simulation data of the bead−spring model, with up to $N = 51$ beads, the maximum number of modes required was found to be $m = 5$. In these cases, it is only possible to obtain an error estimate on λ_η^* due to estimation errors in the fitting parameters in eq 26. The estimation errors in λ_η^* were in the range 1−5%. Notably, the relaxation time found this way has a lesser margin of error and greater accuracy (in terms of scaling with N) than the longest relaxation time λ_1 determined by allowing stretched molecules to relax to equilibrium, which has been used extensively so far.[4,6]

In Table 4, the scaling of λ_η^* with N for various parameter combinations is displayed. These scalings are valid only within the range of N indicated and were used to interpolate at intermediate values of N. The elongational rate at each N is found from $\dot{\epsilon}^* = Wi/\lambda_\eta^*$, for a given choice of Weissenberg number Wi. The relaxation time λ_η obtained in this manner was found to be $\lambda_\eta \approx 1.9\lambda_1$, so that the Weissenberg number used in this study is also ∼1.9 times the Weissenberg number used in ref 8.

Simulations of an ensemble of trajectories are carried out at the values of N shown in Table 3, and the values of $U_{\bar{\eta}R}^+$ obtained at each of these values are extrapolated to the limit $(N-1) \to N_k$, at a fixed fluid Hencky strain $\epsilon = \dot{\epsilon}^* t$. The number of trajectories chosen for a run is typically $\mathcal{O}(10^4)$. Depending on the error of estimation (at 95% confidence), results from more trajectories are added to the saved data so as to obtain reliable extrapolations.

The insensitivity of the extrapolated value of scaled elongational stress growth coefficient $U_{\bar{\eta}R}^+$ to the HI parameter $\tilde{h}^*$ at a solvent quality $z = 1$ and Weissenberg number $Wi = 190$ is shown in Figure 1. Here, the finite N data are extrapolated to $(N-1) \to N_k$, for two different values of $\tilde{h}^*$, and is shown for three different strains experienced by the fluid. Two features to be noted are that (i) while $U_{\bar{\eta}R}^+$, at all the strains shown in Figure 1, is dependent on the choice of $\tilde{h}^*$ at finite N, the extrapolated value is not, and (ii) $U_{\bar{\eta}R}^+$ is independent of $\tilde{h}^*$ both for low strains (coillike) as well as for high strains (rodlike close to full extension). A similar independence from the choice of d^* (through the parameter K) is seen in Figure 2. The parameter-free (independent of $\tilde{h}^*$ and d^*) growth of $U_{\bar{\eta}R}^+$, obtained by carrying out extrapolations over a range of strains, is shown in Figure 3.

The results of carrying out a similar procedure for other solvent qualities, θ-conditions ($z = 0$) and at $z = 3$, are also displayed in Figure 3. In this figure, the $U_{\bar{\eta}R}^+$

Table 4. Approximate "Power Law" Fits for the Relaxation Time λ_η^* for Various Parameter Combinations[a]

set	$z = 0$		$z = 1, K = 1.0$		$z = 1, K = 1.5$		$z = 3, K = 1.0$	
$\tilde{h}^*$	0.19	0.30	0.19	0.30	0.19	0.30	0.19	0.30
m	1.230	1.122	1.309	1.196	1.318	1.219	1.378	1.262
c	1.510	1.844	1.734	2.132	1.561	1.836	1.838	2.275

[a] The dependence of λ_η^* on N is fitted to $\lambda_\eta^* = cN^m$ in the range of $15 \le N \le 51$. The values of c and m for various parameter sets are shown here. The fit is only a guide to interpolate λ_η^* at intermediate values of N and is not reliable for use beyond this range.

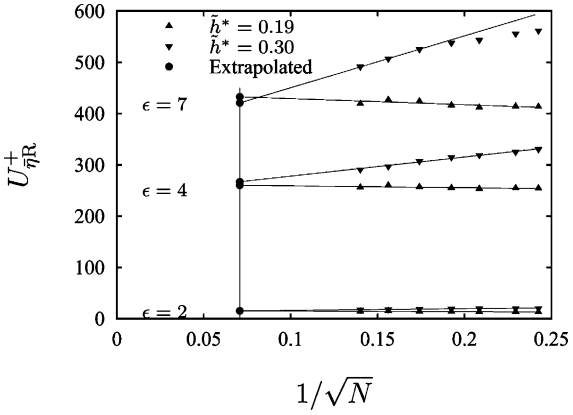

Figure 1. Insensitivity to rescaled HI parameter $\tilde{h}^*$: Extrapolation of simulated finite N to $(N-1) \to N_k$ of the scaled stress growth coefficient $U^+_{\bar{\eta}\mathrm{R}}$ obtained at $N_k = 200$, $z = 1$, and $Wi = 190$ and at three different strains ϵ as indicated. The rescaled HI parameter $\tilde{h}^*$ was kept constant along each data set as indicated in the legend and $K = 1$ for all data. The vertical line corresponds to $N = N_k = 200$. The error bars have not been displayed as they are smaller than the symbol size.

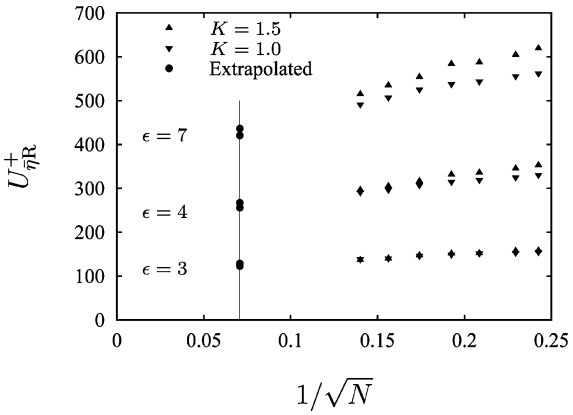

Figure 2. Insensitivity to EV parameter d^*: Extrapolation of the simulated scaled stress growth coefficient $U^+_{\bar{\eta}\mathrm{R}}$ obtained at finite N to N_k at $N_k = 200$, $z = 1$, and $Wi = 190$ and at three different strains ϵ. Here, d^* was varied with two values of K, as indicated above. The rescaled HI parameter was kept constant at $\tilde{h}^* = 0.30$. The vertical line corresponds to $N = N_k = 200$. The error bars have not been displayed as they are smaller than the symbol size.

data below a strain of $\epsilon = 1$ have been omitted, as reliable extrapolations were not obtained for the number of beads N considered. It is interesting to note that, when plotted in terms of $U^+_{\bar{\eta}\mathrm{R}}$, the curves for various solvent qualities apparently collapse to a single curve up to about a strain of $\epsilon \lesssim 3$. At lower strains, the increased rate of growth of the viscosity at a higher solvent quality is offset by the higher R_g^* at equilibrium (see eq 16). However, at larger strains when the

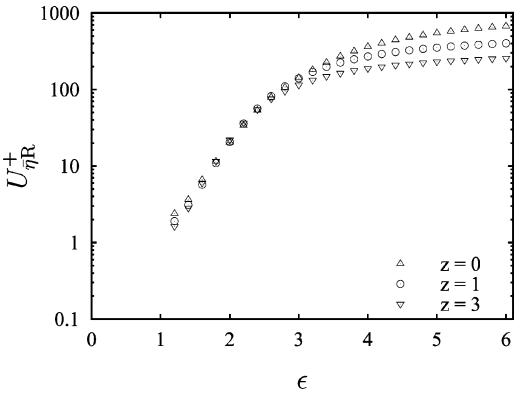

Figure 3. Comparison of the simulated $U^+_{\bar{\eta}\mathrm{R}}$ at three different solvent qualities and at $N_k = 200$ and $Wi = 190$. The interaction parameters have the values $\tilde{h}^* = 0.19$ and $K = 1.0$. The data below $\epsilon = 1$ omitted as reliable extrapolations was not achievable with the finite chain data at hand. The error bars have not been displayed as they are smaller than the symbol size.

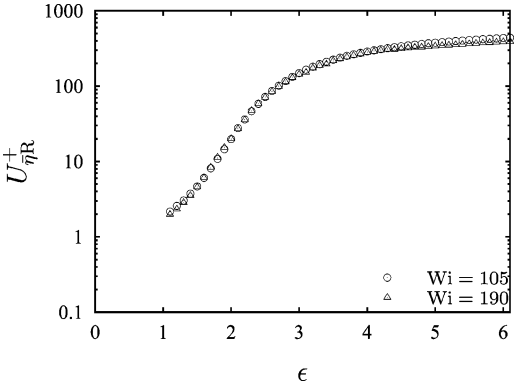

Figure 4. Comparison of the simulated $U^+_{\bar{\eta}\mathrm{R}}$ obtained at two different, showing the growth curve having attained its asymptotic behavior ($Wi \to \infty$) by $Wi = 105$. In both the cases, $N_k = 200$ curve and $z = 1$. The error bars have not been displayed as they are smaller than the symbol size.

molecule is close to fully stretched, EV effects are weak, and it is expected that the elongational viscosity will be independent of the solvent quality. The apparent decrease in $U^+_{\bar{\eta}\mathrm{R}}$ at higher z is due to a higher value of R_g^* at equilibrium, which is used for normalizing the viscosity. This point will be further illustrated in section 4.3.

Simulations carried out at another Weissenberg number, $Wi = 105$, shown in comparison with $Wi = 190$ in Figure 4, indicate that the curves for $Wi = 190$ displayed in Figure 3 are essentially the asymptotic behavior of the stress growth coefficient. A similar observation was made by Doyle and Shaqfeh,[53] who carried out free draining bead−rod simulations and observed that the asymptotic Weissenberg number is around $Wi \sim 60$ (recalculated in terms of λ_η).

In a recent article[22] on predicting the extensional viscosity in polystyrene solutions under θ-conditions, Prabhakar et al. used two different nondimensional ratios to extrapolate the elongational viscosity accumulated for finite N. Prabhakar et al. defined, at low strains, a nondimensional viscosity ratio $\bar{\eta}_p^*$ (distinct from the variable $\bar{\eta}^*$ used here) which was obtained by normalizing the viscosity by bead−rod model parameters, while for higher strains, a variable φ was used, which is the ratio of $\bar{\eta}_p^*$ obtained from the simulations to its value at steady state calculated from an analytical

approximation for a fully stretched bead−spring chain. The justification for using φ was that the ratio φ led to better extrapolations.

In the present work we have used $U^{+}_{\bar{\eta}\mathrm{R}}$ for both low- and high-strain extrapolations. The advantages of using $U^{+}_{\bar{\eta}\mathrm{R}}$ are as follows. In $U^{+}_{\bar{\eta}\mathrm{R}}$, the viscosity is normalized using the equilibrium value of the radius of gyration of the bead−spring chain model. While under θ-conditions and for a chain with FENE springs, the variable $\bar{\eta}^{*}_{p}$ used in ref 22 and $U^{+}_{\bar{\eta}\mathrm{R}}$ differ only by a known multiplicative constant; for a good solvent and springs with other force laws, $U^{+}_{\bar{\eta}\mathrm{R}}$ is the more convenient form to obtain the predictions because (i) there is no necessity to convert expressions from a bead−spring model to a bead−rod model (which, for instance, is not a simple expression for a wormlike chain model) and (ii) it is simpler and "natural" to evaluate, as the radius of gyration is obtained directly after the equilibration run, irrespective of the solvent quality or the force law used. Additionally, we find that even for larger strains the extrapolations in $U^{+}_{\bar{\eta}\mathrm{R}}$ give reliable values, provided we take a large number of trajectories to reduce the error of estimation at each finite N.

An estimate of the computational time required to obtain the theoretical predictions is as follows. The equilibrium runs to estimate the relaxation time scaling for a single parameter set, shown in Table 4, takes about 300 CPU hours on an Intel Pentium 4 CPU 2.4 GHz. The nonequilibrium runs for $Wi = 190$ take about 100 CPU hours on a similar processor for a single parameter set shown in Figure 4.

4.2. Experimental Measurements. In the discussion to follow, the experimentally measured elongational viscosity $\bar{\eta}$ (or stress growth coefficient) will be scaled by the solvent viscosity and plotted as a function of the strain experienced by the fluid, so that the value of $\bar{\eta}/\eta_{\mathrm{s}} \rightarrow 3$ in the limit of zero strain. At low strains several experimental problems can cause uncertainty in the measured value. Some of these have been discussed in ref 10. In addition, for sugar solutions, a skin formation on the surface leads to erroneous force measurement. Use of a thin layer of silicone oil alleviates this problem but does not totally eliminate it. Hence, in the figures to follow, data at low strains have not been displayed.

The measured stress growth coefficient is shown in Figure 5. Here, the scaled coefficient $\bar{\eta}/\eta_{\mathrm{s}}$ has been plotted for the DNA-2 and DNA-5 solutions, described in section 2, subjected to strain rates in the range 5.6−53.4 s^{-1}. As mentioned earlier, these strain rates far exceed the inverse relaxation time of λ-DNA in both the solutions. In terms of the Wi defined with respect to the relaxation time λ_{η} given in Table 2, this corresponds to Wi in the range 610−2245.

The collapse of all the data in Figure 5 onto a unique curve is experimental confirmation of the existence of a limiting asymptotic growth of $\bar{\eta}/\eta_{\mathrm{s}}$ for $Wi \gg 1$. Similar observations were reported in refs 12 and 16. For the DNA-5 solution the limitations in measuring the stresses at low solution viscosities, as discussed in section 2, permitted experiments to be conducted only at a single strain rate. However, the collapse of these data with the other data in Figure 5 confirms that the measured stresses of the DNA-5 solution are also in the asymptotic limit. (Note that for the DNA-5 solution the Weissenberg number corresponds to $Wi = 908$.) The agreement of the growth curves for DNA-2 and DNA-5 solutions in Figure 5 also implies that the λ-DNA has the same solvent quality in both the solutions.

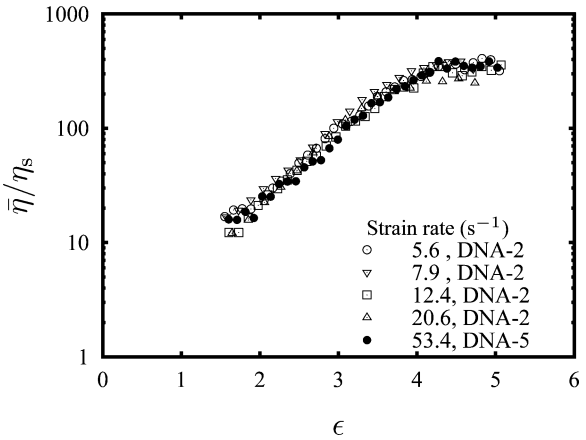

Figure 5. Asymptotic nature of the experimental normalized elongational stress growth coefficient (or elongational viscosity) of a dilute concentration of λ-DNA in solutions labeled DNA-2 and DNA-5, obtained from the filament stretching rheometer. The strain rates are indicated in the legend. The Weissenberg numbers correspond to Wi in the range 610−2245 for DNA-2 and $Wi = 908$ for DNA-5.

4.3. Comparison of Experiments with Predictions from SFG. To apply the SFG method to predict the measurements, we require R^{θ}_{g}, z, and L_0 of λ-DNA at the solvent conditions used in the experiments. As pointed out in ref 8, currently available data for DNA make it difficult to assign values to R^{θ}_{g} and z without a large uncertainty, and values of $R^{\theta}_{\mathrm{g}} = 0.63$ μm, $z = 1$, and $L_0 = 22$ μm (which corresponds to $N_{\mathrm{k}} = 200$) were suggested for YOYO-stained λ-DNA in a sugar solution. Though these values are tentative, pending careful experimental confirmation, they are not inconsistent with observed measurements including that of the extension of DNA in elongational flow. We will consequently assume similar values for these quantities in the present work. It is thought that staining only modifies the persistence length of λ-DNA, and the total number of persistence lengths remains constant.[54] Therefore, assuming the same $N_{\mathrm{k}} = 200$ for a length of 16.5 μm for the unstained DNA, we obtain $R^{\theta}_{\mathrm{g}} = 0.475$ μm from the standard expression for a wormlike chain.[26] In ref 8, a solvent quality of $z = 1$ was suggested for the solution considered by Smith and Chu.[4] This leads to a radius of gyration $R_{\mathrm{g}} = 0.608$ μm (obtained from a swelling ratio of $\alpha_{\mathrm{g}}(z = 1) = 1.28$). Using this, we can obtain the value of the universal ratio $U_{\eta\mathrm{R}}$ (equivalent to Flory's constant):

$$U^{\mathrm{expt}}_{\eta\mathrm{R}} \equiv \frac{[\eta]_0 M/N_{\mathrm{A}}}{\frac{4}{3}\pi {R_{\mathrm{g}}}^3} = 1.27 \pm 0.07 \qquad (27)$$

where we have used the value of $[\eta]_0 = 0.023 \pm 0.01$, obtained from the shear experiments explained in section 2. It is also possible to evaluate the ratio $U_{\eta\mathrm{R}}$ from simulations in the limit of $N \rightarrow \infty$.

$$U^{\mathrm{theo}}_{\eta\mathrm{R}} = \lim_{N\rightarrow\infty} \frac{9}{8}\sqrt{\pi} h^{*} \frac{\lambda^{*}_{\eta}}{{R_{\mathrm{g}}}^{*3}} = 1.3 \pm 0.1 \qquad (28)$$

The theoretical value was obtained by carrying out simulations at $z = 1$ at finite N and extrapolating the

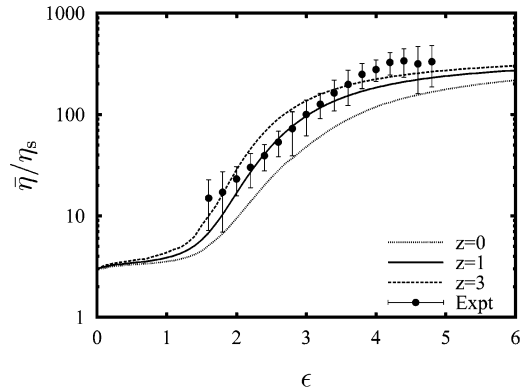

Figure 6. Comparison of theoretical (SFG) predictions of the normalized elongational stress growth coefficient with experimental measurements. The experimental points are averages obtained from the data plotted in Figure 5, with the error bars indicating a 95% confidence interval. The theoretical curves predicted by the SFG scheme are at three solvent qualities (including a θ-solvent with $z = 0$), and $N_k = 200$. Both the experimental and theoretical growth curves are the asymptotic curves for large Wi.

results to the limit $N \to \infty$. Comparing the values of $U_{\eta R}$ obtained from experiments and theory, it is encouraging to note that a radius of gyration of $R_g^\theta = 0.475$ μm and solvent quality of $z = 1$ suggested for the solution used in ref 4 provide a good description of the linear viscoelastic data of the λ-DNA solution used in this work as well. Nevertheless, in the following, we will compare the theoretical predictions of the viscosity growth for three different solvent qualities (theta, $z = 1$, and $z = 3$) with the experimental measurements. The radius of gyration for each of these solvent qualities is obtained by multiplying R_g^θ by the known swelling ratios $\alpha_g(z) = R_g/R_g^\theta$,[37] namely, $\alpha_g(1) = 1.28$ and $\alpha_g(3) = 1.54$.

Since experimental observations correspond to behavior in the asymptotic limit of large Weissenberg numbers, the results of the previous section for $Wi = 190$ can be used for comparison. The scaled elongational viscosity is given in terms of $U^+_{\bar{\eta}R}$ by

$$\frac{\bar{\eta}}{\eta_s} = 3 + \frac{4}{3}\pi {R_g}^3 n_p U^+_{\bar{\eta}R} \tag{29}$$

where $n_p = cN_A/M$ is obtained from the values listed in Table 2.

In Figure 6, the theoretical predictions for the asymptotic stress growth coefficient for three solvent qualities are shown along with the experimental measurements. The experimental points on the plot are averages of the five asymptotic strain rates shown in Figure 5. The influence of solvent quality on the growth of elongational viscosity is clear from this plot. A comparison with the curve at $z = 0$ (θ-conditions) shows that it is essential to include excluded-volume effects to correctly predict the elongational viscosity of DNA solutions. It is also clear that the curve at a solvent quality $z = 1$ best describes the average growth data.

From Figure 3, we noted that for strains up to $\approx$3 the value of $U^+_{\bar{\eta}R}$ is approximately same for all the solvent qualities considered; the difference seen in Figure 6 therefore mainly comes from the equilibrium radius of gyration in eq 29. This provides corroboratory evidence for the value of R_g of λ-DNA. In other words, owing to the "independence" of $U^+_{\bar{\eta}R}$ from the solvent quality at low strains, we can use eq 29 to estimate the equilibrium R_g from the elongational stress measurements. The value $R_g = 0.608$ μm which is required to explain the value of $U^{expt}_{\eta R}$ in eq 27 is also the same value as obtained through the measurements of $\bar{\eta}$.

In the previous section we noted that the solvent quality has an apparently opposite effect in the fully stretched state, viz., a decrease in $U^+_{\bar{\eta}R}$ for higher z. However, from Figure 6, where only the viscosity is plotted, it is clear that for higher strains the effect of solvent quality diminishes as the chain is extended close to its full extension, and the observations made in the previous section are merely due to dividing the viscosity by a factor (R_g) which increases with solvent quality.

Similar to the conclusions made in ref 8, we reiterate here that, although $z = 1$ seems to provide a better agreement with the experiments of linear viscoelasticity and extensional rheology, it should be borne in mind that other combinations of R_g^θ and z which combine to give nearly the same value $R_g = 0.608$ μm under good solvent conditions could lead to similar predictions. It is essential therefore to perform careful experimental measurements to resolve either one of these quantities unambiguously.

5. Conclusion

Elongational stress growth coefficients (or viscosities) of a dilute solution of λ-DNA in pure sugar and sugar + corn-syrup solutions were measured using a filament stretching rheometer. To obtain the corresponding theoretical curves for the growth, it is necessary to include excluded-volume (EV) interactions between parts of the DNA molecule. A recently introduced method to treat EV effects in bead−spring chain models was used in a Brownian dynamics simulation (BDS) framework which also includes hydrodynamic interaction (HI) among the beads. This method not only is capable of providing a parameter-free prediction but also enables the EV interactions to be treated with a known equilibrium measure, which is the solvent quality parameter z.

Using only three equilibrium measures, the radius of gyration at θ-conditions R_g^θ, solvent quality z, and the contour length of λ-DNA L_0, parameter-free predictions of the stress growth coefficient were obtained and compared with the experimental measurements. An equilibrium radius of gyration for λ-DNA of $R_g = 0.608$ μm was found to be consistent with both the linear viscoelastic ratio $U^{expt}_{\eta R}$ (which is equivalent to Flory's constant Φ) and the elongational stress growth coefficient $\bar{\eta}$.

Though existing measurements with DNA do not permit accurate determination of the solvent quality z, this is not insurmountable, given that there are carefully collected experimental results for a few other systems such as that reported in refs 24 and 25. We hope this study motivates cataloguing of quality data for both equilibrium and flow properties, in terms of the solvent quality parameter z.

Acknowledgment. This work has been supported by a grant from the Australian Research Council, under the Discovery-Projects program. The computations were carried out in the facilities provided by the Australian Partnership for Advanced Computation (APAC), the Victorian Partnership for Advanced Computation (VPAC), and the Monash University Engineering faculty Beowulf

Cluster initiative (BC727), and we are grateful for their support.

References and Notes

(1) Doi, M.; Edwards, S. F. *The Theory of Polymer Dynamics;* Clarendon Press: Oxford, 1986.
(2) Volkmuth, W. D.; Austin, R. H. *Nature (London)* **1992**, *358*, 600−602.
(3) Ertaş, D. *Phys. Rev. Lett.* **1998**, *80*, 1548−1551.
(4) Smith, D. E.; Chu, S. *Science* **1998**, *281*, 1335−1340.
(5) Schroeder, C. M.; Shaqfeh, E. S. G.; Chu, S. *Macromolecules* **2004**, *37*, 9242−9256.
(6) Jendrejack, R. M.; de Pablo, J. J.; Graham, M. D. *J. Chem. Phys.* **2002**, *116*, 7752−7759.
(7) Hsieh, C.-C.; Li, L.; Larson, R. G. *J. Non-Newtonian Fluid Mech.* **2003**, *113*, 147−191.
(8) Sunthar, P.; Prakash, J. R. *Macromolecules* **2005**, *38*, 617−640.
(9) Fuller, G. G.; Cathey, C. A.; Hubbard, B.; Zebrowski, B. E. *J. Rheol.* **1987**, *31*, 235−249.
(10) McKinley, G. H.; Sridhar, T. *Annu. Rev. Fluid Mech.* **2002**, *34*, 375−415.
(11) Sridhar, T.; Tirtaatmadja, V.; Nguyen, D. A.; Gupta, R. K. *J. Non-Newtonian Fluid Mech.* **1991**, *40*, 271−280.
(12) Tirtaatmadja, V.; Sridhar, T. *J. Rheol.* **1993**, *37*, 1081−1102.
(13) Szabo, P. *Rheol. Acta* **1997**, *36*, 277−284.
(14) Anna, S. L.; McKinley, G. H.; Nguyen, D. A.; Sridhar, T.; Muller, S. J.; Huang, J.; James, D. F. *J. Rheol.* **2001**, *45*, 83−114.
(15) Anna, S. L.; Rogers, C.; McKinley, G. H. *J. Non-Newtonian Fluid Mech.* **1999**, *87*, 307−335.
(16) Gupta, R. K.; Nguyen, D. A.; Sridhar, T. *Phys. Fluids* **2000**, *12*, 1296−1318.
(17) Smith, D. E.; Babcock, H. P.; Chu, S. *Science* **1999**, *283*, 1724−1727.
(18) Schroeder, C. M.; Teixeira, R. E.; Shaqfeh, E. S. G.; Chu, S. *Macromolecules* **2005**, *38*, 1967−1978.
(19) Bird, R. B.; Curtiss, C. F.; Armstrong, R. C.; Hassager, O. *Dynamics of Polymeric Liquids*, 2nd ed.; John Wiley: New York, 1987; Vol. 2.
(20) Larson, R. G. *J. Rheol.* **2005**, *49*, 1−70.
(21) Zimm, B. H. *J. Chem. Phys.* **1956**, *24*, 269−281.
(22) Prabhakar, R.; Prakash, J. R.; Sridhar, T. *J. Rheol.* **2004**, *48*, 1251−1278.
(23) Louis Barrat, J.; Joanny, J.-F. *Adv. Chem. Phys.* **1996**, *94*, 1−66.
(24) Miyaki, Y.; Fujita, H. *Macromolecules* **1981**, *14*, 742−746.
(25) Hayward, R. C.; Graessley, W. W. *Macromolecules* **1999**, *32*, 3502−3509.
(26) Yamakawa, H. *Modern Theory of Polymer Solutions;* Harper and Row: New York, 1971.
(27) Schäfer, L. *Excluded Volume Effects in Polymer Solutions;* Springer-Verlag: Berlin, 1999.
(28) Fetsko, S. W.; Cummings, P. T. *J. Rheol.* **1995**, *39*, 285−299.
(29) Cifre, J. G. H.; de la Torre, J. G. *J. Rheol.* **1999**, *43*, 339−358.
(30) Li, L.; Larson, R. G. *Rheol. Acta* **2000**, *39*, 419−427.
(31) Liu, S.; Ashok, B.; Muthukumar, M. *Polymer* **2004**, *45*, 1383−1389.
(32) Neelov, I. M.; Adolf, D. B.; Lyulin, A. V.; Davies, G. R. *J. Chem. Phys.* **2002**, *117*, 4030−4041.
(33) Prabhakar, R.; Prakash, J. R. *J. Non-Newtonian Fluid Mech.* **2004**, *116*, 163−182.
(34) Prakash, J. R.; Öttinger, H. C. *Macromolecules* **1999**, *32*, 2028−2043.
(35) Prakash, J. R. *Macromolecules* **2001**, *34*, 3396−3411.
(36) Prakash, J. R. *Chem. Eng. Sci.* **2001**, *56*, 5555−5564.
(37) Kumar, K. S.; Prakash, J. R. *Macromolecules* **2003**, *36*, 7842−7856.
(38) Perkins, T. T.; Smith, D. E.; Chu, S. Single polymers in elongational flows: Dynamic steady-state, and population-averaged properties. In ref 39, pp 283−334.
(39) Nguyen, T. Q., Kausch, H.-H., Eds.; *Flexible Polymer Chains in Elongational Flow: Theory and Experiment*; Springer: Berlin, 1999.
(40) Dubbelboer, R. Extensional rheology of two model polyelectrolytes in dilute solution. Ph.D. Thesis, Monash University, 2003.
(41) Orr, N.; Sridhar, T. *J. Non-Newtonian Fluid Mech.* **1999**, *82*, 203−232.
(42) Szabo, P.; McKinley, G. H. *Rheol. Acta* **2003**, *42*, 269−272.
(43) Öttinger, H. C. *Stochastic Processes in Polymeric Fluids;* Springer: Berlin, 1996.
(44) Marko, J. F.; Siggia, E. D. *Macromolecules* **1995**, *28*, 8759−8770.
(45) Rotne, J.; Prager, S. *J. Chem. Phys.* **1969**, *50*, 4831−4837.
(46) Fixman, M. *Macromolecules* **1981**, *14*, 1710−1717.
(47) Jendrejack, R. M.; Graham, M. D.; de Pablo, J. J. *J. Chem. Phys.* **2000**, *113*, 2894−2900.
(48) Kröger, M.; Alba-Pérez, A.; Laso, M.; Öttinger, H. C. *J. Chem. Phys.* **2000**, *113*, 4767−4773.
(49) Felderhof, B. U.; Deutch, J. M.; Titulaer, U. M. *J. Chem. Phys.* **1975**, *63*, 740−745.
(50) Diaz, F. G.; de la Torre, J. G.; Freire, J. J. *Macromolecules* **1990**, *23*, 3144−3149.
(51) Frenkel, D.; Smit, B. *Understanding Molecular Simulation: From Algorithms to Applications;* Academic Press: San Diego, 1996.
(52) Istratov, A. A.; Vyvenko, O. F. *Rev. Sci. Instrum.* **1999**, *70*, 1233−1257.
(53) Doyle, P. S.; Shaqfeh, E. S. G. *J. Non-Newtonian Fluid Mech.* **1998**, *76*, 43−78.
(54) Quake, S. R.; Babcock, H.; Chu, S. *Nature (London)* **1997**, *388*, 151−154.

MA0511907